IOP Publishing Nanotechnology
Nanotechnology **26** (2015) 464001 (12pp) doi:10.1088/0957-4484/26/46/464001

Tailoring graphene-based electrodes from semiconducting to metallic to increase the energy density in supercapacitors

Jenel Vatamanu, Xiaojuan Ni, Feng Liu and Dmitry Bedrov

Department of Materials Science & Engineering, University of Utah, USA

E-mail: d.bedrov@utah.edu

Received 6 July 2015, revised 6 September 2015
Accepted for publication 30 September 2015
Published 29 October 2015

Abstract

The semiconducting character of graphene and some carbon-based electrodes can lead to noticeably lower total capacitances and stored energy densities in electric double layer (EDL) capacitors. This paper discusses the chemical and electronic structure modifications that enhance the available energy bands, density of states and quantum capacitance of graphene substrates near the Fermi level, therefore restoring the conducting character of these materials. The doping of graphene with p or n dopants, such as boron and nitrogen atoms, or the introduction of vacancy defects that introduce zigzag edges, can significantly increase the quantum capacitance within the potential range of interest for the energy storage applications by either shifting the Dirac point away from the Fermi level or by eliminating the Dirac point. We show that a combination of doping and vacancies at realistic concentrations is sufficient to increase the capacitance of a graphene-based electrode to within 1 μF cm^{-2} from that of a metallic surface. Using a combination of *ab initio* calculations and classical molecular dynamics simulations we estimate how the changes in the quantum capacitance of these electrode materials affect the total capacitance stored by the open structure EDL capacitors containing room temperature ionic liquid electrolytes.

Keywords: supercapacitors, quantum capacitance, modeling

(Some figures may appear in colour only in the online journal)

1. Introduction

In the context of increasing demand for electricity-based energy storage, experimental and theoretical research into various electrolytes at charged surfaces has increased significantly in the last decade. In particular, the electric double layer supercapacitors (EDLC) have been considered as promising energy storage technologies [1–3]. In these devices the energy storage is achieved due to non-Faradaic processes, i.e., due to purely electrostatic interactions between the charged (porous) electrode and the electrolyte. This confers supercapacitors unique advantages such as fast charging rates, high delivered power, and a virtually unlimited number of charge-discharge cycles. In EDLCs, the electrolyte typically consists of a room temperature ionic liquid (RTIL) or organic solvent with high salt concentration. As for the electrode, carbon-based materials are often preferred because they are relatively cheap, can be fabricated to have a highly porous structure (hence a high specific surface area) and are very versatile to further chemical functionalization. However, some carbon-based electrodes can show semiconducting properties leading to lower electronic conductivity and lower capacitance. For example, electrodes based on single graphene sheets or some nanotubes can show semiconducting character [4]. Nanoporous electrodes such as, for example, carbide derived carbons (CDC), while being electronically conductive, can show a strong dependence of conductivity on the processing conditions and the resulting structural elements comprising these electrodes, indicating that the electronic properties in these materials are locally heterogeneous [5]. This can be a disadvantage in energy storage applications because it diminishes the stored energy densities.

If the quantum effects are accounted for, the total capacitance of an electrode (C) can be modeled as two capacitors connected serially [6]: (i) a capacitor representing the quantum capacitance of the system (C_Q) and (ii) a capacitor representing the classical EDL capacitance (C_{EDL}):

$$\frac{1}{C} = \frac{1}{C_Q} + \frac{1}{C_{EDL}}. \quad (1)$$

The EDL capacitance (C_{EDL}) originates from the processes of electrolyte rearrangement near the electrode surface as a response to the charge (or potential) applied on the electrode surface. If the potential (or charge) is applied on the electrode surface, the electrolyte will typically restructure near the surface forming alternating layers of counter- and co-ions and hence leading to an oscillating space charge distribution near the electrode. According to atomistic simulations [7] as well as atomic force microscopy [8, 9] and x-ray reflectometry [10, 11] experiments, such multilayer structures can extend for up to 6 nm from the electrode surface. Note that the interfacial layer can be overcharged, i.e., it can contain more counter-charge than the charge on the electrode surface, and this excess counter-charge in the interfacial layer is compensated by the subsequent ion layers of the multilayer structure. The resulting magnitude and the dependence of the electrode capacitance on the electrode potential will be determined by such complex multilayer electrolyte ordering near the surface. However, as it has been shown in our previous simulations, the structural/charge correlations in the EDL within 2 nm from the electrode surface can quantitatively explain all the features observed in the EDL differential capacitance (DC) as a function of electrode potential [12]. For many commonly-used RTIL-based electrolytes the EDL capacitance on metallic, atomically flat surfaces ranges between 4 and 6 μF cm^{-2}, as shown by a series of simulations [7, 12–18] and experiments [19–23].

The quantum capacitance (C_Q), on the other hand, originates from the quantum effects in the electrode material. A grounded classical planar conductor completely screens out the electrostatic field generated by a charge from penetration to the other side of the plane. However, for a 2D electronic gas in a quantum well there can be a partial penetration of the electrostatic field. Luryi [6] introduced the concept of the quantum capacitance in order to model with an equivalent circuit (equation (1)) the partial penetrability of the electrostatic field through a 2D electron gas in a quantum well. The appearance of C_Q is a consequence of the Pauli principle of filling out the energetic states with fermions and therefore it is quantified by the Fermi–Dirac distribution of the electrons over the available energy states. The C_Q is important in electronic nanodevices because it affects the transconductance of the field-effect transistors [6, 24–26]. Also, the negative local quantum capacitance, that can occur if there is a positive charge feedback (and is achievable, for example, in ferroelectrics [27] or in graphene nanoribbons [28]), can be employed in the design of 'smart gates' for nanocircuits. In the context of energy storage devices, C_Q is receiving increasing attention because electrode materials with a high C_Q near Fermi level increase the stored energy density. However, as shown by experiments [29] and *ab initio* numerical calculations [30–32], the C_Q for graphene has a U-shape dependence on the local gate potential varying between ≈1 and 10 μF cm^{-2} in a typical potential range from −0.4 to +0.4 V. Note that the local potential gate is not the electrode potential but instead it is a potential drop associated with the quantum capacitor serially connected with the EDL capacitor. These values of C_Q are comparable in magnitude with the C_{EDL} and hence can significantly influence the total capacitance of the electrode.

In this work we investigate the influence of the electrode structure on the total capacitance of the open structure electrode/electrolyte systems using a combined *ab initio* DFT and classical molecular dynamics (MD) simulation approach. We show that the semiconducting character of graphene (quantified by the C_Q) significantly changes the magnitude and the shape of the electrode DC, particularly near the potential of zero charge (PZC). We discuss the structural modifications of graphene layers that can restore their conducting character. This could be achieved either by shifting the band structures from the Fermi level (via e.g. doping) such that an increase in the density of states (DOS) and the energy bands become available at and near the Fermi level, or by completely modifying the symmetry of graphene (via generating vacancy defects) which eliminates the Dirac point and generates large DOS at the Fermi level. We show that further increase of C_Q, and hence the total capacitance, is possible if the electrode modification depends on its polarity. For example, doping of graphene layers with n-type impurities (such as N atoms) on the positive electrode and with the p-type impurities (such as B atoms) on the negative appears to optimize the C_Q both on the positive and negative plates, respectively.

2. Simulation methods

2.1 Ab initio calculations

The *ab initio* computations were performed utilizing the VASP package [33]. The electronic structure of pristine, doped or vacancy-defected graphene sheets were calculated using the projector augmented wave (PAW) method [34] for the interaction between core and valence electrons and the Perdew–Burke–Ernzerhof (PBE) functional based on the generalized gradient approximation (GGA) [35] for the exchange-correlation interaction. The kinetic energy cut-off of 400 eV and 24 × 24 × 1 k-points were used. The computations were performed in two steps: in the first step, the structure was relaxed to the minimum energy geometry, then the electronic properties, density of states (DOS) and the band structure (BS) were calculated for the equilibrated structure. The DOS were computed on a grid with energy steps of 0.02 eV. For the graphene nanoribbons we computed the spin-polarized DOS for parallel and antiparallel configurations of spins at the opposite edges [36, 37]. The C_Q was calculated using obtained DOS, taking into account the 2D symmetry as derived in references [24, 30, 31]. As in [30], we

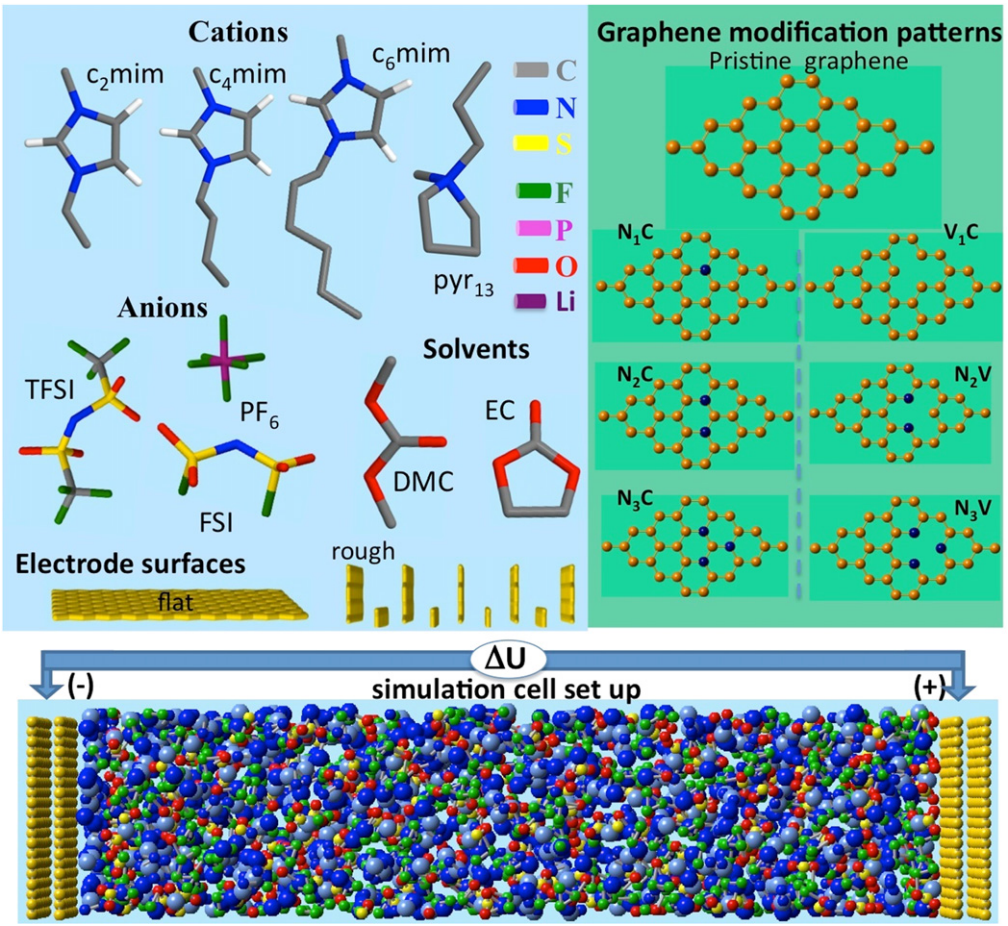

Scheme 1. Schematic illustration of the chemical structure of the ions and the solvent molecules comprising electrolytes, the electrode geometries for classical simulations, the graphene patterns studied with *ab initio* computations, and the simulation cell setup.

assumed that the local gate voltage ϕ_G rigidly shifts the electrochemical potential μ of graphene by $e\phi_G$. The size of the simulation cell for the pristine and doped graphene consisted of 32 atoms. The doped graphene was generated from the pristine graphene configuration by replacing some carbon atoms either with vacancies [38] (V) or with B or N atoms [39] such that the following patterns were generated: X_nC, X_nV, with X = B or N and n = 1–3. To investigate the role of vacancies, the carbon atoms were removed such that zigzag edges were generated in graphene layers comprised of 32, 50 or 72 atoms. Snapshots of configurations investigated by DFT calculations are shown in scheme 1.

2.2 Classical MD simulations

Classical MD simulations were utilized to calculate the EDL structure and the classical EDL capacitance (C_{EDL}). In these simulations the electrode was approximated as a classical conductor, in other words, the EDL capacitance was approximated from the electrolyte response next to a conducting surface. A constant electrostatic potential was imposed on the electrode surface utilizing a method originally described in references [40, 41]. Specifically, the charges on electrode atoms (assumed to be Gaussian distributed with a width of 0.5 Å) [41, 42] were calculated such that the electrode charge distribution minimizes the total electrostatic interaction energy of the system. The minimized energy function incorporates the standard electrostatic term $\Sigma\Sigma q_i q_j erf(\varepsilon r_{ij})/r_{ij}$, where i and j are the indices of electrode atoms, as well as the Gaussian charge self-energy term and the work $-\Sigma q_i \varphi_i$ required to build electrode charges q_i at the electrode surface at a potential φ_i. In this method the charge on each electrode atom i can fluctuate during simulations in response to changes in the electrolyte EDL structure. Additional details about this approach are described in references [17, 18, 43–46].

The simulation cells contained two electrodes and electrolyte between them. The electrodes were represented by either two or three layers of graphene oriented with the atomically flat basal plane toward the electrolyte or the edge plane of graphite comprising the offset of the graphene layers relative to each other, as illustrated in scheme 1. Several electrolytes have been considered, including RTILs comprising 1-butyl-3-alkylimidazolium ($C_n$mim) and N-methyl-N-propylpyrrolidinium (pyr_{13}) cations and hexafluorophosphate ($[PF_6]$), bis(fluorosulfonyl)imide (FSI), and bis(trifluoromethanesulfonyl)imide (TFSI) anions as well as ethylene carbonate (EC)/dimethyl carbonate (DMC) (3:7) mixture with $LiPF_6$ salt. The electrolyte phase was represented by either 120–200 ionic pairs for RTILs or by 114

molecules of EC, 256 molecules of DMC and 31 $LiPF_6$ pairs. These amounts of electrolyte were sufficient to create a separation between electrodes of about 11–20 nm, therefore allowing a sufficient amount of bulk electrolyte to separate the EDLs formed at the electrodes. The RTILs were modeled using the force fields described in [12] for [C_4mim][PF6], in [7] for [$C_n$mim][FSI], in [14] for [$C_n$mim][TFSI], in [47] for [pyr_{13}][FSI] RTILs and in [48] for EC/DMC/$LiPF_6$ electrolyte. Note that RTIL electrolytes were modeled using a nonpolarizable mixed atomistic and united atom model while simulations of the EC/DMC/$LiPF_6$ system employed a fully atomistic, polarizable APPLE&P force field [48]. The polarizability of this electrolyte was represented classically with induced dipoles computed via self-consistent iterations. An illustration of the typical simulation setup and the molecules comprising electrolytes are also shown in scheme 1.

The long-range electrostatic interactions were calculated with the Ewald summation method adapted for the 2D geometry [49, 50]. The reciprocal part of the Ewald summation was handled with an efficient SPME method for the 2D symmetry proposed by Kawata and co-workers [51–54]. The short-range interactions (the van der Waals and the real part of the SPME) were calculated within a spherical cut-off of 10 Å. A reversible multiple-time step algorithm [55] was utilized to integrate the equations of motions as follows. The forces from bonds, bends, and out-of-plane deformations were computed every $\tau/10$, the forces from dihedrals and forces due to nonbonded interactions (van der Waals and the real part of electrostatic interactions) within a cutoff radius of 7.5 Å were updated every $\tau/2$, and the remaining nonbonded forces (i.e., the van der Waals and electrostatic interactions within the 10.0 Å cut off and the reciprocal part of SPME) were computed every τ, where the timescale τ was 3 fs for the EC/DMC/$LiPF_6$ system and 5 fs for the systems with RTIL electrolytes. The electrode charges were updated every 50τ. Each system was simulated at 10–20 different applied potential differences between the electrodes in the range between 0 and 6 V. A typical length of the simulation trajectory was between 10 and 40 ns depending on the mobility of bulk electrolyte near electrode surface. The temperature of the simulations of systems with RTIL electrolytes was 393 K while the EC/DMC/$LiPF_6$ system was simulated at 453 K. The temperature was controlled with Nosé–Hoover chain thermostats [56].

Using the charge distribution across the asymmetry direction averaged over simulation trajectories, the corresponding screened Poisson potential was calculated using a numerical integration of the 1D-Poisson equation. The difference in the Poisson potential between bulk electrolyte and electrode surface defined the EDL potential (U_{EDL}). The U_{EDL} corresponding to uncharged electrodes defined the potential of zero charge (*PZC*). The electrode potential of a conducting electrode (V_e) is then the difference between the U_{EDL} and the *PZC*, $V_e = U_{EDL}$-*PZC*.

2.3 Combined analysis

As mentioned above, the total electrode capacitance (C) can be calculated using equation (1). The total potential drop (V_a) between the electrode and the bulk electrolyte (that can be represented as serially connected classical and quantum capacitors) is then the sum of the local gate potential (V_g) on the capacitor representing the quantum effects and the potential drop on the 'classical' (EDL) capacitor, $V_a = V_g + V_e = V_g + U_{EDL}$-*PZC*. The *PZC* and the U_{EDL} were taken from MD simulations near conducting surfaces while the local (quantum) gate potential was approximated as $V_g = -(E\text{-}E_{Fermi})/e$ from the DFT calculations [31]. The V_g was computed based on the total electrode charge, i.e., both quantum and classical capacitors were assumed to have the same charge because they are serially connected, as described in [31]. Other approximations utilized here were similar to those in previous Paek *et al* works [30, 31, 57–60]. Due to limited electrolyte electrochemical stability, the total electrode potential in the EDL supercapacitors typically varies within the range −3 to +3 V. Note that the C_Q increases sharply with potential. Therefore a typical range of the local gate voltage V_g of interest for the energy storage applications is within $|V_g| < 0.5$ V. The following *differential capacitances* will be discussed in the paper: the EDL capacitance C_{EDL} obtained from MD simulations on a metallic surface, the quantum capacitance of the electrode C_Q extracted from DFT predicted DOS, and the total capacitance of a semiconducting electrode C defined by equation (1). It is important to recall that our approach neglects the role of electrolyte proximity on the band structure of the electrode. In other words, the bands were assumed to be affected only by the structural impurities in graphene. Also we approximate the capacitance associated with electrolyte reordering near a semiconducting electrode to be the same as for a metallic electrode. Similar approximations were previously utilized by Paek and co-workers [30, 31].

3. Results and discussion

Figure 1 shows the band structure, DOS and C_Q for a single pristine graphene layer. Because of the presence of the Dirac point in the band structure at the K-point (figure 1(a)), the DOS has a U-shape dependence on the energy and a minimum at the Fermi level. As a result of such DOS dependence, the C_Q also has a minimum at the Fermi level and therefore a U-shaped dependence on the local gate voltage. Although at $|V_g| > 1$ V, the C_Q becomes higher than 25 μF cm^{-2} at lower V_g, which are more relevant for the energy storage applications, and the C_Q is smaller or comparable to the C_{EDL} for typical electrolytes. Previous simulations [15] and experiments [19, 21] probed whether C_{EDL} near flat conducting electrodes for typical RTILs varies between 4.0–5.5 μF cm^{-2}. However, the C_Q of a single graphene sheet has a dramatic drop near *PZC*. Therefore the semiconducting character of graphene can generate a significant drop in the total electrode capacitance, especially at low electrode potentials, as

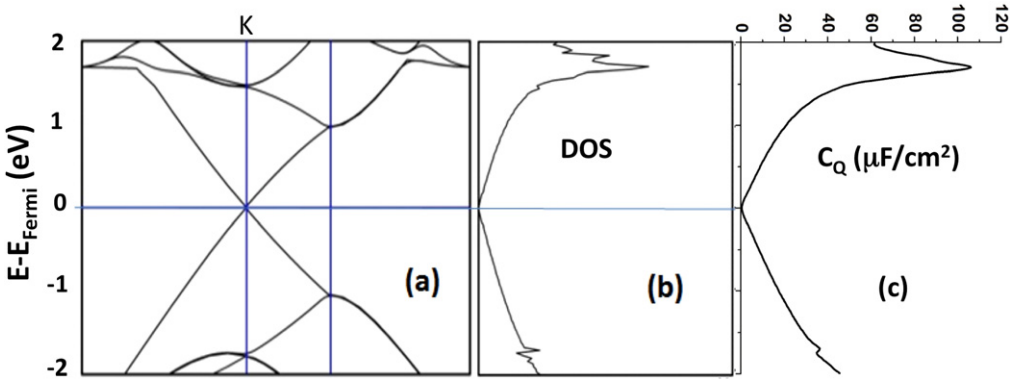

Figure 1. The band structure (a), the DOS (b) and the quantum capacitance (c) for the pristine graphene layer as a function of the energy level.

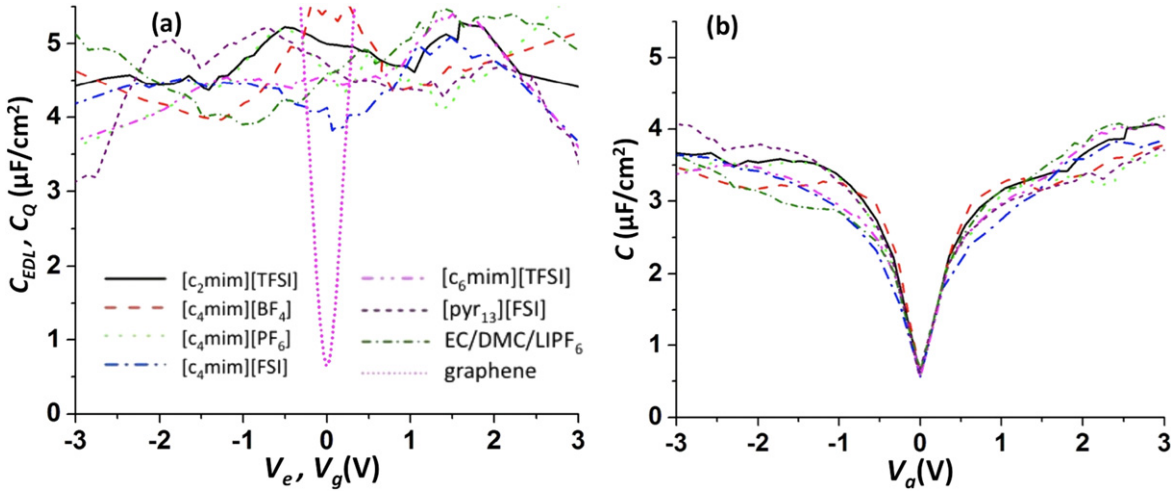

Figure 2. (a) The EDL capacitances as a function of potential for several commonly utilized RTILs and for EC/DMC/$LiPF_6$ electrolyte obtained from MD simulations assuming that the electrode surface is a classical conductor. For comparison, the quantum capacitance of one graphene layer is also shown as a function of local gate voltage V_g. (b) The estimated total capacitance of electrolyte near one graphene layer as a function of electrochemical potential V_a and determined using equation (1).

illustrated in figure 2 where C_{EDL}, C_Q and C are compared for several systems with atomically flat electrodes. It can be seen that despite some variations in the C_{EDL} dependence on the electrode potential for different electrolytes considered, near *PZC* the C is dominated by the small value of C_Q and all systems show a qualitatively similar total capacitance dependence as a function of electrode voltage.

The C_Q drop near the Fermi level is due to the unavailability of the DOS and has important theoretical implications. Basic theoretical models of EDL typically assume a constant electrostatic potential across the electrode surface, i.e., they treat the electrode as a classical conductor. Such EDL models can predict for dilute solutions of ions a minimum (or U-shaped) C_{EDL} at low voltages based entirely on classical (i.e., steric) considerations of ion packing: for diluted ions there is sufficient space near the surface for the counterions to accumulate as the driving force (the electrostatic potential acting on the ions) increases. The EDL models that account for the excluded volume of ions can predict the U-shaped C_{EDL} at low voltages both for diluted ion solutions and for RTILs [61, 62]. However, as shown in figure 2, the semiconducting character of graphene and its influence on the C_Q can also generate a pronounced minimum and the U-shape capacitance at low voltages. The minimum in the C_{EDL} obtained from MD simulations at the conducting surface is significantly less pronounced than the feature generated by the quantum effects in graphene. It is therefore possible that in systems with carbon-based electrodes, the minimum in the total differential capacitance (C) near *PZC* has primarily quantum, rather than classic, origin. In the remainder of this paper we will explore the possibilities of restoring high values of C_Q in graphene-based structures. We will consider several modifications of graphene-based electrodes and their influence on the C_Q and the total capacitance.

3.1 Non-chemical factors

First, let us consider a few factors that do not change the underlying graphene structure, i.e., the temperature, compression/extension, and number of graphene layers. The DOS for these three modifications are shown in figure 3. The experimental literature sometimes shows contradicting trends regarding the influence of temperature on C measured in RTIL-based electrolytes on carbon-based electrodes. For

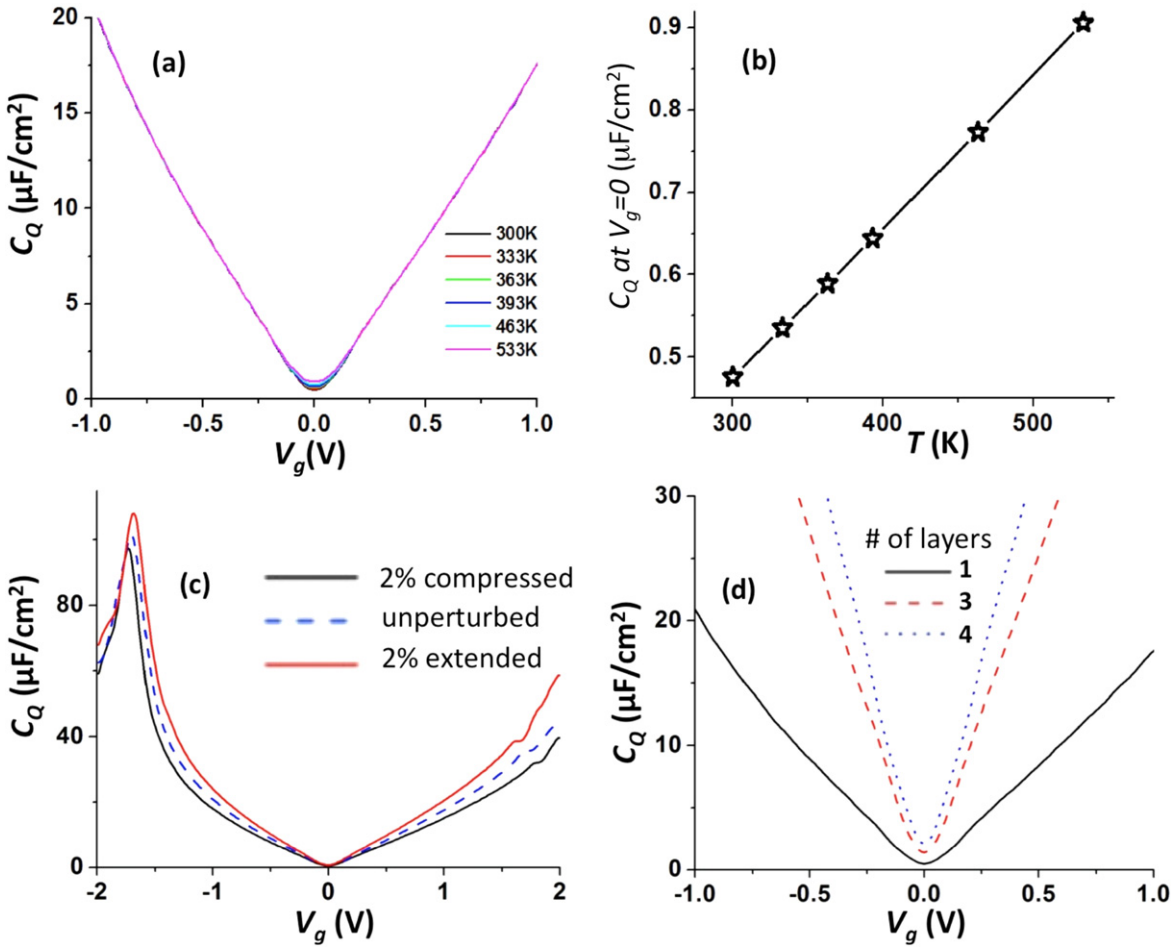

Figure 3. (a) The influence of temperature on C_Q. (b) Temperature dependence of C_Q at zero V_g. (c) The role of mechanical distortion of graphene on C_Q. (d) The influence of additional graphene layer on C_Q.

example, references [63–65] showed an increase in the capacitance with temperature while other experiments [19, 21] and simulations [13] found negligible or only a slight decrease in the total capacitance with increasing temperature. Figure 3(a) shows that the C_Q cannot contribute (within the temperature range of practical interest for the energy storage) significantly to the C temperature dependence. The C_Q has only a weak dependence on temperature near zero gate voltage. Specifically at the Dirac point, a change in temperature from 300 K to 533 K increases the C_Q from 0.47 to 0.95 μF cm^{-2} which is expected from the Fermi–Dirac distribution (figure 3(b)). Above the $\pm$0.1 V gate voltage the C_Q becomes essentially independent of temperature.

We also found that straining (compression or extension) the graphene layer up to 2% only slightly changes the C_Q (figure 3(c)). Also the location of the minimum in C_Q near the Dirac point remains unaffected as a function of applied strain. Interestingly, even if the stresses generated by such mechanical modifications are large, the C_Q remains largely unaffected. Similar results were observed in another *ab initio* study for graphene sheets under uniaxial and biaxial strains [32].

In order to understand how the mutual influence of multiple graphene layers changes the capacitance, we computed the C_Q for electrodes comprised of one, two, three and four layers of graphene arranged in the ABAB stacking and separated at 4.1, 4.3 and 4.0 Å, respectively. These interlayer separation distances were determined based on the crystal structure optimization procedure from VASP. Figure 3(d) shows that the C_Q increases with the increase in the number of graphene layers. However, increasing the number of layers in order to increase the capacitance is not an efficient route to optimize the energy density in supercapacitors, because it leads to an increase in the electrode mass/volume without increasing the surface area accessible to electrolyte. To maximize the specific surface area, the graphene layers need to be exfoliated as much as possible, i.e., a layer of graphene should preferably have both faces in contact with electrolyte. Indeed, the reverse Monte Carlo technique [66–68] as well as classical MD simulations [69] indicated that in experimentally prepared CDC electrodes [70] which showed relatively large gravimetric and volumetric capacitances, the walls of the nanopores are very thin with only one or two graphene-like layers comprising the walls. Therefore to preserve the high specific surface area per mass of the electrode it is necessary to consider other ways to alter the electronic properties of carbon-based nanostructured electrodes. In the next section we examine chemical

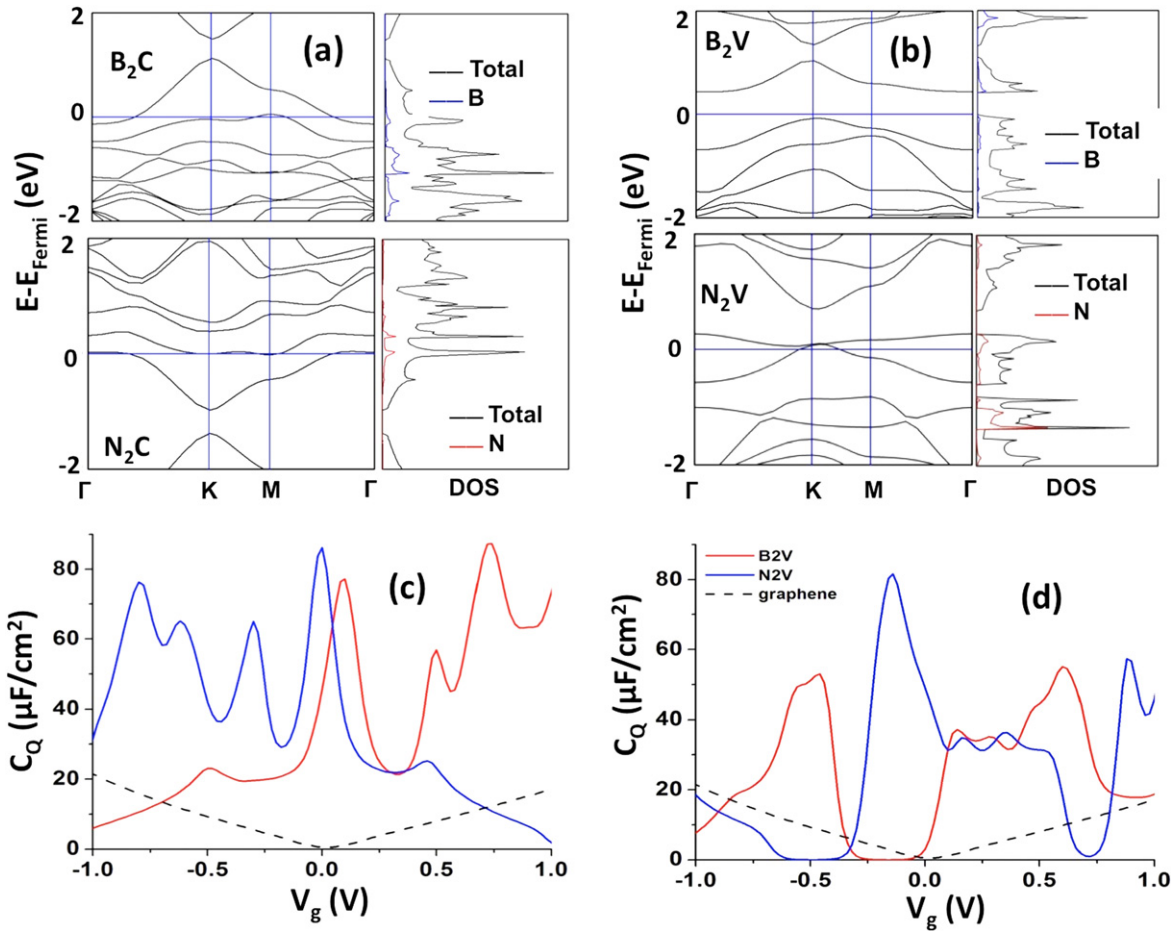

Figure 4. The band structure and the density of states for (a) B_2C and N_2C and (b) B_2V and N_2V patterns. Panels (c) and (d) are the corresponding quantum capacitances. The dashed lines in panels (c) and (d) are the C_Q for the pristine graphene and are shown for comparison.

modifications of a single layer of graphene that lead to an increase in its metallicity.

3.2 Chemical modifications

We have examined doping patterns and dopant concentrations that can increase the C_Q near the Fermi level. Note that recent advances in chemical doping of graphene with nitrogen [71–76], boron [77–81] or metal [82–84] atoms, generation of vacancy defects [85], or its functionalization [86–88] with other chemical groups showed that carbon-based electrodes are chemically versatile, allowing a substantial modification of their chemical and electronic structure. Shown in figure 4(a) are the band structure and DOS for the N_2C and B_2C doping patterns. As already mentioned, the pristine graphene has a Dirac point which generates low DOS near the Fermi level and therefore smaller values of C_Q at zero local gate voltage V_g. If the graphene is doped with the p- or n-type impurities the electrons are subtracted or added to the system. This adds an energy gap at the corresponding K-point in pristine graphene and, importantly, it shifts this gap from the Fermi level. In the case of the p-dopant (B atoms) the gap moves by as much as 1 eV into the conduction band while for the n-dopants (N atoms) the energy gap is shifted by 1 eV into the valence band (figure 4(a)). In other words, the minimum in the DOS and C_Q is no longer located at the Fermi level and instead there is a large increase in DOS near the Fermi level for doped graphene. This leads to a large increase in C_Q at the gate voltages below 0.8 V (see figure 4(c)). Taking into account that a typical operating potential difference for the energy storage applications ($\Delta U = 2.5$–5 V), the relatively small values of C_{EDL} on the flat surfaces (4–6 μF cm^{-2}) for common RTILs, and the fact that C_Q has a sharp dependence on V_g, we do not expect that the gate voltage can exceed $|0.5\,\text{V}|$ for typical supercapacitors with RTIL electrolytes. Therefore, in order to increase the electrode capacitance, it is sufficient to design doping that would move the band gap away from the Fermi level by about 0.5 eV. Clearly, with such doping at certain values of V_g an energy gap will be observed at the negative electrode for the p-dopants and at the positive electrode for the n-dopants. This would lower the C_Q at the corresponding voltages, however this would only happen at very large electrode voltages which commonly falls outside of the electrochemical stability of typical electrolytes.

The introduction of the vacancy defects can also significantly change the DOS and the C_Q of the graphene layers. If the vacancies are generated such that they create zigzag edges they increase the metallic character of graphene. The

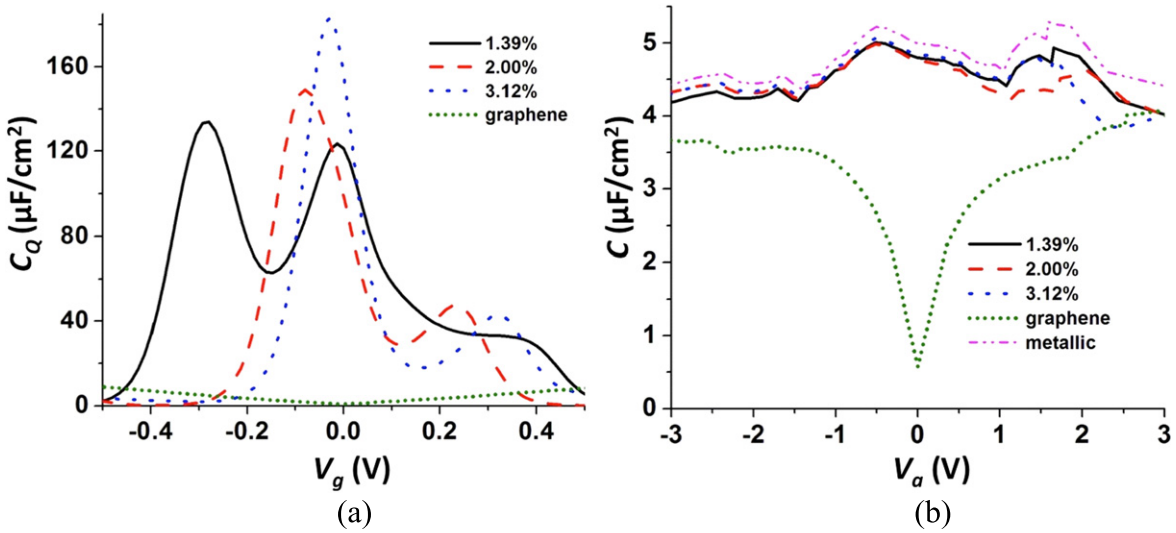

Figure 5. (a) The quantum capacitance of graphene containing vacancy defects as a function of gate voltage and vacancy percentage. (b) The corresponding estimated total C for electrodes with vacancies. The capacitances for semiconducting pristine graphene and the metallic electrode are also shown for comparison.

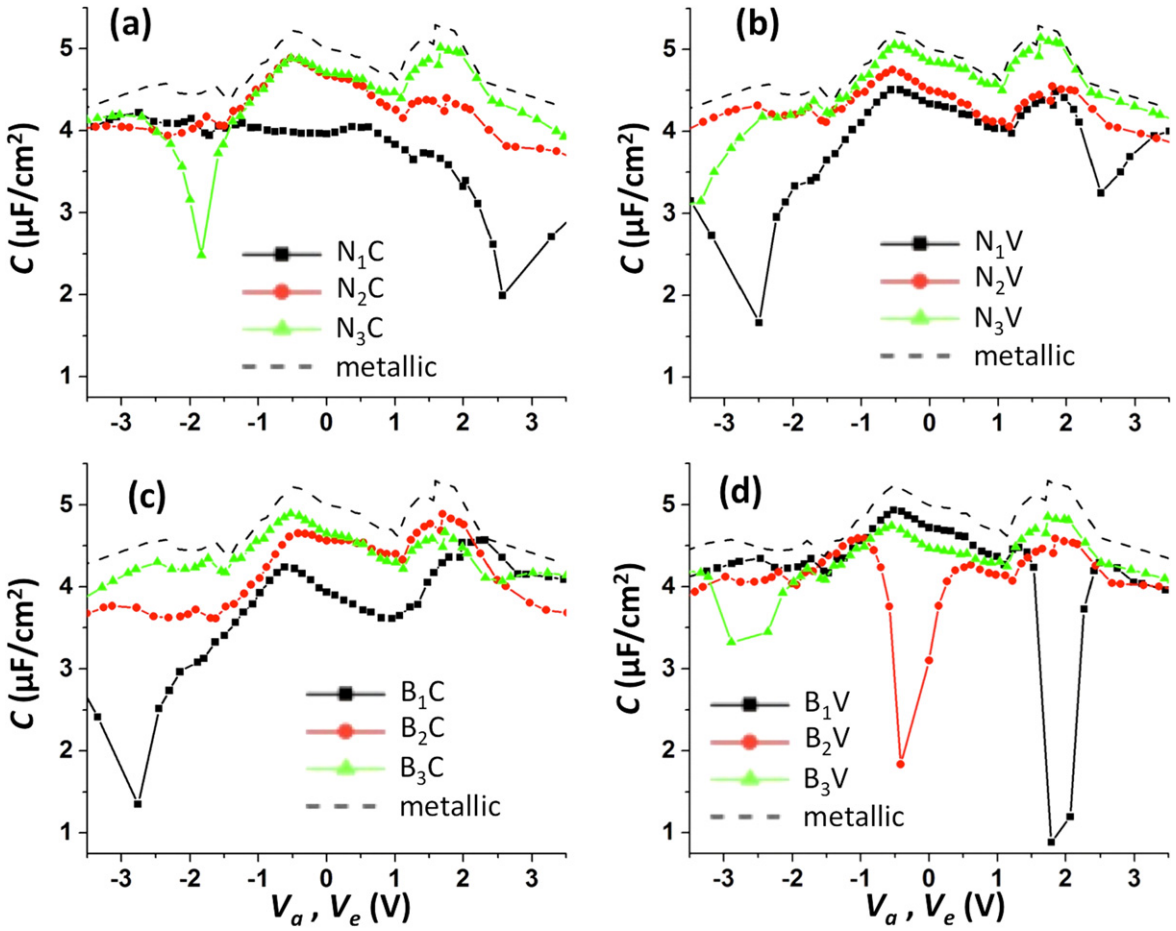

Figure 6. The total C obtained using equation (1) for various doping patterns of graphene and [$c_2$mim][TFSI] electrolyte as a function of electrochemical potential V_a. The dashed line is the C for an electrode modeled as a classical conductor plotted as a function of V_e.

C_Q near the Fermi level has a different shape compared to the pristine or doped graphene, i.e., it shows a pronounced maximum for the C_Q which leads to a substantial improvement in the total capacitance as shown in figure 5. As expected, the maximum is more pronounced for the system with the higher density of vacancies. Such behavior of DOS for graphene can be understood from the fact that the coupling between the pz orbital of the carbon atom neighboring

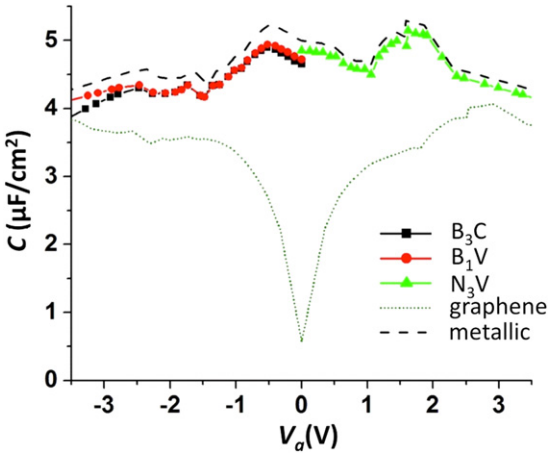

Figure 7. The total capacitance for optimal doping patterns for each electrode and [$c_2$mim][TFSI] electrolyte. For comparison, the estimated C for the same electrolyte on a pristine layer of graphene (dotted line) and near a metallic electrode (dashed line) are shown for comparison. The doped and pristine graphene are represented as a function of V_a, while the C for the metallic electrode is represented as a function of V_e. The *PZC* was substracted out from these potential scales.

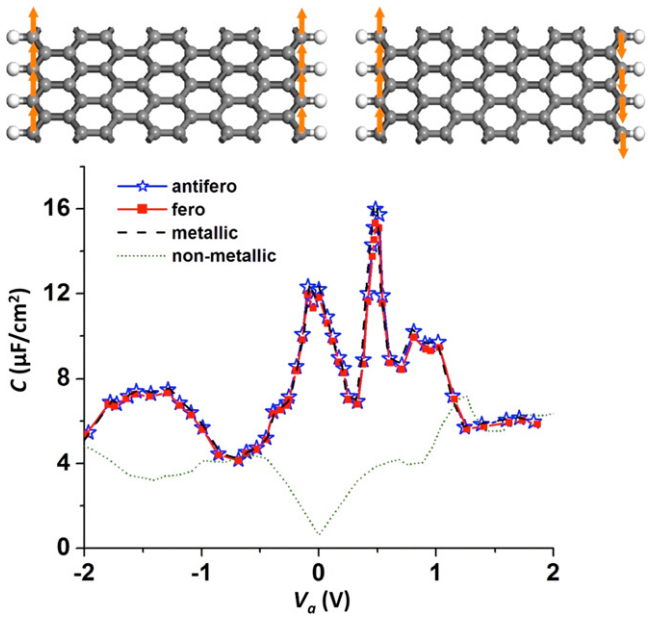

Figure 8. The influence of zigzag (metallic) edges on the total capacitance.

the vacancy and the sp2 orbitals introduces nonequivalent spin states that destroy the Dirac point [89, 90].

Figure 6 shows the influence of the doping and the vacancies on the coupling of C_Q with C_{EDL} and the resulting total capacitance C. In this figure we show the total capacitance for the [$c_2$mim][TFSI] electrolyte near a metallic surface (dash line), the pristine graphene, and the modified graphene structures. The presence of the energy gaps in the graphene band structures generates large drops in the capacitance at certain voltages. For example, the C generated by the N_3C pattern, while it looks very close to the metallic electrode case at positive voltages, has a sharp drop at around −1.8 V. This means that at that voltage the electrode will not accommodate additional charge upon electrode potential increase due to the unavailability of states for the electrons at that particular voltage. Similarly, the N_1C pattern generates C with a significant drop at 2.5 V. Combining vacancies with doping can further increase the capacitance as compared to pure doping. Figures 4(b), (d) show DOS and C_Q while figures 5(b), (d) show the total capacitance for the patterns that combine doping and vacancies. For example, the N_3V pattern generates C very close to a metallic surface in the potential range between −2.2 V and +3.5 V. However, below −2.2 V the N_2V pattern modification outperforms the N_3V. The boron doping B_1C outperforms the denser doped patterns of B_2C and B_3C at the positive surface above +2 V. However, below +2 V the B_2C and B_3C generate larger capacitances. On the negative electrode, the denser doping B_3C generates capacitances essentially close to the metal surface. Introducing vacancies in the B-doped graphene has an undesired effect of generating low C near *PZC* for B_2V and around +2.0 V for B_1V. In turn, the B_3V generates large capacitances at the positive electrode and only slightly lower (between 3 to 4 μF cm^{-2}) at the negative electrode. Taking these aspects into account we surmise that it might be possible to use different doping patterns for electrodes with different polarities in order to optimize the C_Q. For example, figure 7 shows a couple of examples with optimal patterns for the positive and negative electrodes that in combination with each other result in a total capacitance which is similar to those expected from the corresponding systems with metallic electrodes.

The above comparison of the total capacitance for different electrode surface patterns was presented for atomically flat electrode surfaces with the basal plane of graphene exposed to electrolytes. However, it is often the case that the electrode surfaces are atomically corrugated either due to surface restructuring or the preparation process [91]. Furthermore, for energy storage applications, rough electrode surfaces may be desired because they can generate larger C_{EDL}, as has been demonstrated by several simulations [92–95] and experiments [22, 96, 97]. Therefore we also examined the role of graphene edges for the electrodes with atomically rough surfaces. The structure of the termination edges is very important in determining the electronic structure and therefore the shape of the DOS and C_Q [98]. For example, the zigzag edges are metallic while the armchair edges are semiconducting [99–101]. We have considered a nanoribbon with metallic (zigzag) edges with a size of 7.38 Å along the periodic direction and a width of 7.90 Å along the nonperiodic direction. For such nanoribbons we computed the spin polarized DOS. The edges were terminated with H atoms. Note that depending on the spin distribution at the two edges of a nanoribbon, two limiting cases are possible: antiferromagnetic states where the spins are antiparallel and ferromagnetic states where the spins are parallel. The antiferromagnetic state was energetically more stable

with about 0.3 meV $Å^{-1}$ compared to the ferromagnetic one. The total DOS of each state was a summation of the spin-up and the spin-down polarized DOS. The resulting C_Q generated by these edges was combined with the C_{EDL} obtained from MD simulations for this type of electrode surfaces and the estimate of the overall C (obtained using equation (1)) is shown in figure 8. Note that the C_{EDL} for such surfaces is significantly different from those obtained on the basal plane graphite. On the rough surfaces the C_{EDL} dependence on the electrode potential can show multiple-peak dependence with very large peaks near *PZC* as shown in figure 8. The nonmetallic edges (such as armchair ones) can reduce the total capacitance in a similar way as shown for a graphene layer, because they also have a minimum in the DOS near the Fermi level. However, if the electrode surface is filled with metallic zigzag edges as discussed above, then the C_Q will be sufficiently large to generate the total electrode capacitance very similar to those generated by metallic surfaces (see figure 8).

4. Conclusions

An implication of the semiconducting character of graphene is the unavailability of the energy bands near the Dirac point and therefore low density of states near the Fermi level. As a result, the pristine graphene has a low quantum capacitance near the Fermi level which, in turn, can cause a pronounced U-shaped dependence of the total differential capacitance on the electrode potential. In this work we showed that doping patterns and structural modifications could be introduced to graphene substrate in order to increase its quantum capacitance and make it more suitable for energy storage applications. Two types of electronic modifications can enhance the C_Q: (i) a shift of the Dirac point from the Femi level achievable via doping and making the energy bands and the DOS available at low gate voltage, and (ii) inducing asymmetries that destroy the Dirac point and generate bands (and DOS) near the Fermi level by introducing vacancy defects.

The C_Q of graphene can be enhanced by doping it with N and B and by generating vacancies. The maximum graphene doping density that is experimentally possible, to date, which is similar to that in our simulated B_1C/V or N_1C/V patterns, can generate electrode capacitances within about 1 $\mu F\,cm^{-2}$ (on average) from the capacitances obtained on the ideal conductor of similar surface topography. Higher doping densities can generate total capacitances within 0.2–0.3 $\mu F\,cm^{-2}$ of the metallic electrode over essentially the entire potential range corresponding to the window of electrochemical stability of typical electrolytes. The doping of graphene-based electrodes can be asymmetric with respect to the electrode polarity: the positive electrode should be doped with the n-type impurities (e.g., N_3V pattern) while the negative electrode should be doped with the p-type impurities (e.g., B_1V or B_3C patterns).

The best route to generating high C_Q is to prepare electrodes with a high density of zigzag edges. Rough edges provide dual beneficial effect. On the one hand, they enhance the EDL capacitance via the classical effect of surface roughness when their roughness dimensions are similar to the ions' sizes, as shown in references [7, 12, 93], and on the other hand, the electronic structure of the zigzag rough edges allows them to behave essentially as conductors. Furthermore, the rough edges have an advantage of increasing (almost doubling) the capacitance in the subnanometer pores as compared to smooth surface pores of similar widths [102].

Acknowledgments

The authors would like to acknowledge the University of Utah MRSEC (National Science Foundation Grant #DMR 11-21252) for the support through the seed grant program and the University of Utah Center for High Performance Computing for generous allocations of computational resources. XN and FL would also like to acknowledge the support by the Department of Energy EBS program (Grant DE-FG02-04ER46148).

References

[1] Simon P and Gogotsi Y 2008 *Nat. Mater.* **7** 845
[2] Xiong G, Meng C, Reifenberger R G, Irazoqui P P and Fisher T S 2014 *Electroanalysis* **26** 30
[3] Vatamanu J and Bedrov D 2015 *J. Phys. Chem. Lett.* **6** 3594
[4] Ramuz M P, Vosgueritchian M, Wei P, Wang C, Gao Y, Wu Y, Chen Y and Bao Z 2012 *ACS Nano* **6** 10384
[5] Dryfe R *et al* 2014 *Faraday Discuss.* **172** 117
[6] Luryi S 1988 *Appl. Phys. Lett.* **52** 501
[7] Hu Z, Vatamanu J, Borodin O and Bedrov D 2014 *Electrochim. Acta* **145** 40
[8] Zhang X, Zhong Y-X, Yan J-W, Su Y-Z, Zhang M and Mao B-W 2012 *Chem. Commun.* **48** 582
[9] Hayes R, Borisenko N, Tam M K, Howlett P C, Endres F and Atkin R 2011 *J. Phys. Chem.* C **115** 6855
[10] Yamamoto R, Morisaki H, Sakata O, Shimotani H, Yuan H, Iwasa Y, Kimura T and Wakabayashi Y 2012 *Appl. Phys. Lett.* **101** 053122
[11] Mezger M, Ocko B M, Reichert H and Deutsch M 2013 *Proc. Natl Acad. Sci. USA* **110** 3733
[12] Hu Z, Vatamanu J, Borodin O and Bedrov D 2013 *Phys. Chem. Chem. Phys.* **15** 14234
[13] Vatamanu J, Xing L, Li W and Bedrov D 2014 *Phys. Chem. Chem. Phys.* **16** 5174
[14] Vatamanu J, Borodin O, Bedrov D and Smith G D 2012 *J. Phys. Chem.* C **116** 7940
[15] Vatamanu J, Borodin O and Smith G D 2010 *J. Am. Chem. Soc.* **132** 14825
[16] Merlet C, Salanne M, Rotenberg B and Madden P A 2013 *Electrochim. Acta* **101** 262
[17] Xing L, Vatamanu J, Borodin O, Smith G D and Bedrov D 2012 *J. Phys. Chem.* C **116** 23871
[18] Vatamanu J, Borodin O and Smith G D 2011 *J. Phys. Chem.* C **116** 1114
[19] Druschler M, Borisenko N, Wallauer J, Winter C, Huber B, Endres F and Roling B 2012 *Phys. Chem. Chem. Phys.* **14** 5090
[20] Alam M T, Islam M M, Okajima T and Ohsaka T 2007 *J. Phys. Chem.* C **111** 18326
[21] Cannes C, Cachet H, Debiemme-Chouvy C, Deslouis C, de Sanoit J, Le Naour C and Zinovyeva V A 2013 *J. Phys. Chem.* C **117** 22915

[22] Costa R, Pereira C M and Silva A F 2015 *Electrochim. Acta* **167** 421
[23] Gomes C, Costa R, Pereira C M and Silva A F 2014 *RSC Adv.* **4** 28914
[24] John D L, Castro L C and Pulfrey D L 2004 *J. Appl. Phys.* **96** 5180
[25] Yan Q, Huang B, Yu J, Zheng F, Zang J, Wu J, Gu B-L, Liu F and Duan W 2007 *Nano Lett.* **7** 1469
[26] Huang B, Yan Q, Zhou G, Wu J, Gu B-L, Duan W and Liu F 2007 *Appl. Phys. Lett.* **91** 253122
[27] Salvatore G A, Lattanzio L, Bouvet D, Stolichnov I, Setter N and Ionescu A M 2010 *Appl. Phys. Lett.* **97** 053503
[28] Reiter R, Derra U, Birner S, Terrés B, Libisch F, Burgdörfer J and Stampfer C 2014 *Phys. Rev.* B **89** 115406
[29] Xia J, Chen F, Li J and Tao N 2009 *Nat. Nanotechnology* **4** 505
[30] Paek E, Pak A J, Kweon K E and Hwang G S 2013 *J. Phys. Chem.* C **117** 5610
[31] Paek E, Pak A J and Hwang G S 2013 *J. Electrochem. Soc.* **160** A1
[32] Wood B C, Ogitsu T, Otani M and Biener J 2014 *J. Phys. Chem.* C **118** 4
[33] Hafner J 2008 *J. Comput. Chem.* **29** 2044
[34] Blöchl P E 1994 *Phys. Rev. B* **50** 17953
[35] Perdew J P, Burke K and Ernzerhof M 1996 *Phys. Rev. Lett.* **77** 3865
[36] Yu D, Lupton E, Gao H J, Zhang C and Liu F 2008 *Nano Res.* **1** 497
[37] Yu D, Lupton E, Liu M, Liu W and Liu F 2008 *Nano Res.* **1** 56
[38] Liu W, Wang Z F, Shi Q W, Yang J and Liu F 2009 *Phys. Rev.* B **80** 233405
[39] Chen L, Hu H, Ouyang Y, Pan H Z, Sun Y Y and Liu F 2011 *Carbon* **49** 3356
[40] Siepmann J I and Sprik M 1995 *J. Chem. Phys.* **102** 511
[41] Reed S K, Lanning O J and Madden P A 2007 *J. Chem. Phys.* **126** 084704
[42] Vatamanu J, Borodin O and Smith G D 2010 *Phys. Chem. Chem. Phys.* **12** 170
[43] Pastewka L, Järvi T T, Mayrhofer L and Moseler M 2011 *Phys. Rev.* B **83** 165418
[44] Wang Z, Yang Y, Olmsted D L, Asta M and Laird B B 2014 *J. Chem. Phys.* **141** 184102
[45] Kiss P T, Sega M and Baranyai A 2014 *J. Chem. Theory Comput.* **10** 5513
[46] Golze D, Iannuzzi M, Nguyen M-T, Passerone D and Hutter J 2013 *J. Chem. Theory Comput.* **9** 5086
[47] Vatamanu J, Borodin O and Smith G D 2011 *J. Phys. Chem.* B **115** 3073
[48] Borodin O 2009 *J. Phys. Chem.* B **113** 11463
[49] Heyes D M 1994 *Phys. Rev.* B **49** 755
[50] Heyes D M 1984 *Phys. Rev.* B **30** 2182
[51] Kawata M and Mikami M 2001 *Chem. Phys. Lett.* **340** 157
[52] Kawata M, Mikami M and Nagashima U 2002 *J. Chem. Phys.* **116** 3430
[53] Kawata M, Mikami M and Nagashima U 2001 *J. Chem. Phys.* **115** 4457
[54] Kawata M and Nagashima U 2001 *Chem. Phys. Lett.* **340** 165
[55] Martyna G J, Tuckerman M E, Tobias D J and Klein M L 1996 *Mol. Phys.* **87** 1117
[56] Hoover W G 1985 *Phys. Rev.* A **31** 1695
[57] Paek E, Pak A J and Hwang G S 2015 *J. Chem. Phys.* **142** 024701
[58] Paek E, Pak A J and Hwang G S 2013 *J. Phys. Chem.* C **117** 23539
[59] Pak A J, Paek E and Hwang G S 2013 *Phys. Chem. Chem. Phys.* **15** 19741
[60] Pak A J, Paek E and Hwang G S 2014 *Carbon* **68** 734
[61] Kornyshev A A 2007 *J. Phys. Chem.* B **111** 5545
[62] Oldham K B 2008 *J. Electroanal. Chem.* **613** 131
[63] Silva F, Gomes C, Figueiredo M, Costa R, Martins A and Pereira C M 2008 *J. Electroanal. Chem.* **622** 153
[64] Costa R, Pereira C M and Silva F 2010 *Phys. Chem. Chem. Phys.* **12** 11125
[65] Alam M T, Masud J, Islam M M, Okajima T and Ohsaka T 2011 *J. Phys. Chem.* C **115** 19797
[66] Pikunic J, Clinard C, Cohaut N, Gubbins K E, Guet J-M, Pellenq R J M, Rannou I and Rouzaud J-N 2003 *Langmuir* **19** 8565
[67] Zetterström P, Urbonaite S, Lindberg F, Delaplane R G, Leis J and Svensson G 2005 *J. Phys.: Condens. Matter* **17** 3509
[68] Jain S K, Pellenq R J M, Pikunic J P and Gubbins K E 2006 *Langmuir* **22** 9942
[69] Merlet C, Péan C, Rotenberg B, Madden P A, Daffos B, Taberna P L, Simon P and Salanne M 2013 *Nat. Commun.* **4** 2701
[70] Largeot C, Portet C, Chmiola J, Taberna P-L, Gogotsi Y and Simon P 2008 *J. Am. Chem. Soc.* **130** 2730
[71] Wang H, Maiyalagan T and Wang X 2012 *ACS Catal.* **2** 781
[72] Lu Y-F, Lo S-T, Lin J-C, Zhang W, Lu J-Y, Liu F-H, Tseng C-M, Lee Y-H, Liang C-T and Li L-J 2013 *ACS Nano* **7** 6522
[73] Lv R *et al* 2012 *Sci. Rep.* **2** 586
[74] Geng D, Yang S, Zhang Y, Yang J, Liu J, Li R, Sham T-K, Sun X, Ye S and Knights S 2011 *Appl. Surf. Sci.* **257** 9193
[75] Wang L, Sofer Z, Luxa J and Pumera M 2014 *J. Mater. Chem.* C **2** 2887
[76] Wen Z, Wang X, Mao S, Bo Z, Kim H, Cui S, Lu G, Feng X and Chen J 2012 *Adv. Mater.* **24** 5610
[77] Lazar P, Zboril R, Pumera M and Otyepka M 2014 *Phys. Chem. Chem. Phys.* **16** 14231
[78] Sheng Z-H, Gao H-L, Bao W-J, Wang F-B and Xia X-H 2012 *J. Mater. Chem.* **22** 390
[79] Gebhardt J, Koch R J, Zhao W, Höfert O, Gotterbarm K, Mammadov S, Papp C, Görling A, Steinrück H P and Seyller T 2013 *Phys. Rev.* B **87** 155437
[80] Ju L *et al* 2014 *Nat. Nanotechnology* **9** 348
[81] Zhao L *et al* 2013 *Nano Lett.* **13** 4659
[82] Toh R J, Poh H L, Sofer Z and Pumera M 2013 *Chem.—An Asian J.* **8** 1295
[83] Giovanni M, Poh H L, Ambrosi A, Zhao G, Sofer Z, Sanek F, Khezri B, Webster R D and Pumera M 2012 *Nanoscale* **4** 5002
[84] Kong X-K, Chen C-L and Chen Q-W 2014 *Chem. Soc. Rev.* **43** 2841
[85] Meyer J C, Kisielowski C, Erni R, Rossell M D, Crommie M F and Zettl A 2008 *Nano Lett.* **8** 3582
[86] Georgakilas V, Otyepka M, Bourlinos A B, Chandra V, Kim N, Kemp K C, Hobza P, Zboril R and Kim K S 2012 *Chem. Rev.* **112** 6156
[87] Craciun M F, Khrapach I, Barnes M D and Russo S 2013 *J. Phys.: Condens. Matter.* **25** 423201
[88] Boukhvalov D W and Katsnelson M I 2009 *J. Phys.: Condens. Matter.* **21** 344205
[89] Yang G M, Zhang H Z, Fan X F and Zheng W T 2015 *J. Phys. Chem.* C **119** 6464
[90] Fan X F, Liu L, Wu R Q, Peng G W, Fan H M, Feng Y P, Kuo J L and Shen Z X 2010 *J. Phys.: Condens. Matter.* **22** 046001
[91] Jänsch T, Wallauer J and Roling B 2015 *J. Phys. Chem.* C **119** 4620
[92] Vatamanu J, Cao L, Borodin O, Bedrov D and Smith G D 2011 *J. Phys. Chem. Lett.* **2** 2267
[93] Xing L, Vatamanu J, Smith G D and Bedrov D 2012 *J. Phys. Chem. Lett.* **3** 1124
[94] Ho T A and Striolo A 2013 *J. Chem. Phys.* **139** 204708

[95] Tazi S, Salanne M, Simon C, Turq P, Pounds M and Madden P A 2010 *J. Phys. Chem.* B **114** 8453
[96] Randin J P and Yeager E 1971 *J. Electrochem. Soc.* **118** 711
[97] Tang M, Miyazaki K, Abe T and Newman J 2012 *J. Electrochem. Soc.* **159** A634
[98] Pak A J, Paek E and Hwang G S 2014 *J. Phys. Chem.* C **118** 21770
[99] Han M Y, Özyilmaz B, Zhang Y and Kim P 2007 *Phys. Rev. Lett.* **98** 206805
[100] Barone V, Hod O and Scuseria G E 2006 *Nano Lett.* **6** 2748
[101] Son Y-W, Cohen M L and Louie S G 2006 *Phys. Rev. Lett.* **97** 216803
[102] Vatamanu J, Vatamanu M and Bedrov D 2015 *ACS Nano* **9** 5999